Nanoscale

PAPER

View Article Online
View Journal | View Issue

Cite this: *Nanoscale*, 2023, **15**, 19577

Electrocatalytic nitrate-to-ammonia conversion on CoO/CuO nanoarrays using Zn–nitrate batteries†

Shanshan Chen,[a] Gaocan Qi,[b]* Ruilian Yin,[c] Qian Liu,[d] Ligang Feng,[e] Xincai Feng,[f] Guangzhi Hu,[g] Jun Luo,[f] Xijun Liu*[h] and Wenxian Liu*[c]

Received 18th October 2023,
Accepted 15th November 2023

DOI: 10.1039/d3nr05254k

rsc.li/nanoscale

$Zn–NO_3^-$ batteries can generate electricity while producing NH_3 in an environmentally friendly manner, making them a very promising device. However, the conversion of NO_3^- to NH_3 involves a proton-assisted 8-electron ($8e^-$) transfer process with a high kinetic barrier, requiring high-performance catalysts to realize the potential applications of this technology. Herein, we propose a heterostructured CoO/CuO nanoarray electrocatalyst prepared on a copper foam (CoO/CuO-NA/CF) that can electrocatalytically and efficiently convert NO_3^- to NH_3 at low potential and achieves a maximum NH_3 yield of 296.9 μmol h^{-1} cm^{-2} and the Faraday efficiency (FE) of 92.9% at the −0.2 V *vs.* reversible hydrogen electrode (RHE). Impressively, $Zn–NO_3^-$ battery based on the monolithic CoO/CuO-NA/CF electrode delivers a high NH_3 yield of 60.3 μmol h^{-1} cm^{-2}, FE_{NH3} of 82.0%, and a power density of 4.3 mW cm^{-2}. This study provides a paradigm for heterostructured catalyst preparation for the energy-efficient production of NH_3 and simultaneously generating electrical energy.

1. Introduction

Ammonia (NH_3) is considered one of the most promising carbon-free energy carriers and is widely used in various fields, including manufacturing fertilizers, plastic production, and disinfection.[1,2] NH_3 has traditionally been synthesized using the Haber–Bosch (H–B) process, which operates at high temperatures and pressures, consumes a significant amount of energy, and also generates CO_2 emissions.[3,4] The electrochemical method for ammonia synthesis has the advantages of mild reaction conditions and no pollution.[5–7] Recently, various nitrogen-containing substances, such as nitrogen (N_2), nitric oxide (NO), nitrite (NO_2^-), and nitrate (NO_3^-), have been investigated as potential nitrogen sources for the electrochemical synthesis of NH_3.[8–10] In particular, NO_3^-, as one of the most common global groundwater pollutant, has a high solubility in water and possesses a low N–O bond energy (204 kJ mol^{-1}).[11–17] Therefore, electrocatalytic NO_3^- reduction reaction (NO_3RR) provides a sustainable alternative for NH_3 production while treating NO_3^- containing wastewater.[18] Additionally, coupling NO_3RR with the redox reaction of Zn/Zn^{2+} to form a $Zn–NO_3^-$ battery is also capable of simultaneously generating electricity.[19] Unfortunately, this promising "three birds with one stone" technology is still in its infancy due to the lack of high-performance NO_3RR electrocatalysts.

Transition metals have garnered significant interest in electrochemical redox reactions owing to their advantages of low price, abundance, and adjustable activity.[20–32] In particular, Cu-based catalysts have been widely studied as NO_3RR electrocatalysts owing to their high conductivity and efficient inhibiting effect on hydrogen evolution.[33–37] Unfortunately, Cu-based catalysts have drawbacks of low activity and unsatisfactory stability for NO_3RR. Moreover, the intermediates produced by NO_3RR (*NO_2, *NO, *N, *etc.*) cannot be hydrogenated in time due to the poor adsorption capacity of H* on copper, resulting in a slow kinetic process of the reaction.[38] The construction of heterostructures allows the coupling capabilities of various species, optimizing the energetics of the reaction intermediates on active sites, thus enhancing the intrinsic

[a]*Institute for New Energy Materials & Low-Carbon Technologies, School of Materials Science and Engineering, Tianjin University of Technology, Tianjin 300384, China*
[b]*School of Materials Science and Engineering, Tianjin University of Technology, Tianjin 300384, China. E-mail: gaocanqi@tjut.edu.cn*
[c]*College of Materials Science and Engineering, Zhejiang University of Technology, Hangzhou 310014, China. E-mail: liuwx@zjut.edu.cn*
[d]*Institute for Advanced Study, Chengdu University, Chengdu 610106, Sichuan, China*
[e]*School of Chemistry and Chemical Engineering, Yangzhou University, Yangzhou 225002, China*
[f]*ShenSi Lab, Shenzhen Institute for Advanced Study, University of Electronic Science and Technology of China, Longhua District, Shenzhen 518110, China*
[g]*Institute for Ecological Research and Pollution Control of Plateau Lakes, School of Ecology and Environmental Science Yunnan University, Kunming 650091, China*
[h]*State Key Laboratory of Featured Metal Materials and Life-cycle Safety for Composite Structures, MOE Key Laboratory of New Processing Technology for Nonferrous Metals and Materials, School of Resources, Environment and Materials, Guangxi University, Nanning 530004, China. E-mail: xjliu@gxu.edu.cn*

† Electronic supplementary information (ESI) available. See DOI: https://doi.org/10.1039/d3nr05254k

catalytic performance.[39–42] For instance, Liu *et al.*[43] demonstrated that the heterogeneous interface between $Cu_{2+1}O$ and Ag accelerates the electron transfer between the components and synergistically enhances the NO_3RR performance. Deng *et al.*[44] prepared a heterostructure of CoP/TiO_2 nanoarrays on titanium plates, which can effectively improve the electrocatalytic NO_3RR activity. Theoretical calculations show that the hetero-interface can induce the charge redistribution of CoP and TiO_2 and optimize the adsorption-free energy of the intermediates. Remarkably, Co species have high intrinsic activity for nitrate reduction and are considered potential metal species to improve the catalytic activity with high NH_3 selectivity at negative potentials.[45–47] Coupling Co-based compounds and Cu-based components to construct heterostructure catalysts has the potential to simultaneously enhance NO_3RR activity and selectivity, enabling high-performance $Zn–NO_3^-$ batteries.[48,49]

Herein, heterostructured CoO/CuO nanoarrays were prepared on the surface of Cu foam through an electrochemical deposition-thermal treatment method. The introduction of CoO sites into CuO catalysts could modulate the electronic structure of CuO and significantly improve its NO_3RR performance. Specifically, the CoO/CuO-NA/CF catalyst achieved the maximum NH_3 yield of 296.9 μmol h^{-1} cm^{-2} and FE of 92.9% at −0.2 V *vs.* RHE. More importantly, the developed CoO/CuO-NA/CF catalyst could be used as a cathode in $Zn–NO_3^-$ battery to obtain an optimal NH_3 yield of 60.3 μmol h^{-1} cm^{-2}, an FE of 82.0%, as well as a high power density of 4.3 mW cm^{-2}.

2. Experimental section

2.1. Chemicals and materials

Copper foam (CF, Thickness 1.5 mm, 99.9%) was purchased from Innokai Technology Co., Ltd. Nitric acid (65%–68%) was purchased from Sinopharm Chemical Reagent Co., Ltd. Potassium hydroxide (95%) was purchased from Meryer (Shanghai) Chemical Technology Co., Ltd. $CoCl_2$ (anhydrous, 97%) was purchased from Sinopharm Chemical Reagent Co., Ltd.

2.1.1 Synthesis of a $Cu(OH)_2$ nanoarray ($Cu(OH)_2$-NA/CF).. $Cu(OH)_2$-NA/CF was synthesized *via* the anodic oxidation method. First, a piece (2 cm × 3 cm) of CF was immersed in 30 mL of 3 M HNO_3 aqueous solution to get rid of the oxidized layer, followed by washing with deionized water and ethanol. Subsequently, the as-treated CF and the graphite rod were used as an anode and a cathode, respectively, in 60 mL of 1.0 M KOH aqueous solution and 1.5 V was applied; the electrolysis lasted for 20 min wherein the tan CF gradually turned blue. Finally, after washing with ethanol and deionized water, it was dried under an infrared light.

2.1.2 Synthesis of CuO-NA/CF. The as-prepared $Cu(OH)_2$-NA/CF was heated in a tube furnace at 200 °C under an Ar atmosphere for 2 h at the rate of 1 °C min^{-1} in order to avoid excessive oxidation of CF. After that, it was allowed to cool naturally, and a brownish-black electrode of CuO-NA/CF was successfully synthesized.

2.1.3 Synthesis of CoO/CuO-NA/CF. CoO/CuO-NA/CF was synthesized *via* the electrodeposition method. The as-prepared $Cu(OH)_2$-NA/CF and the graphite rod were used as anodes and cathodes, respectively, in 60 mL of 30 mM $CoCl_2$ aqueous solution, When −1 V voltage was applied, the electrolysis lasted for 900 s. Finally, after washing with ethanol and deionized water, it was dried under an infrared light to obtain $Co–Cu(OH)_2$. The $Co–Cu(OH)_2$ was heated in a tube furnace at 200 °C under an Ar atmosphere for 2 h at the rate of 1 °C min^{-1}. After that, it was allowed to cool naturally, and a brownish-black electrode of CoO/CuO-NA/CF was successfully synthesized.

2.2. Characterization

SEM, TEM, HAADF-STEM images, and EDX mappings of the samples were obtained using an FEI Talos F200X S/TEM with a field-emission gun at 200 kV. XRD patterns were obtained using an X-ray diffractometer (Rigaku SmartLab) from 10 to 90 at a scan rate of 10 min^{-1} with Cu Kα radiation (λ = 0.154598 nm). XPS spectra were collected on a Thermo Scientific K-alpha XPS system (Thermo Fisher Scientific, UK) with the Al Kα radiation as the X-ray source. The absorbance data of the spectrophotometer were collected using a UV-vis spectrophotometer. The liquid products were characterized using the Avance III HD 400 MHz NMR instrument.

2.3. Electrochemical measurements

Electrochemical NO_3RR tests were performed in an H-type reactor separated by a Nafion 117 membrane. The electrolyte was 0.5 M NaOH (with or without 250 ppm NO_3^-–N) solution in compartments. The Hg/HgO electrode and Pt foil (1 × 1 cm^2) were used as the reference and counter electrodes, respectively. CF, CuO-NA/CF, and CoO/CuO-NA/CF were used as working electrodes. The NO_3RR linear sweep voltammetry (LSV) curves were obtained at a sweep rate of 10 mV s^{-1}. All the

Wenxian Liu

Wenxian Liu received his bachelor's degree in applied chemistry from Tianjin University in 2012. He completed his Ph.D. with Prof. Junfeng Liu at the College of Science at Beijing University of Chemical Technology in 2017. After that, he joined the College of Materials Science and Engineering at Zhejiang University of Technology. His research interests focus on the preparation of advanced nanocatalysts for electrochemical energy storage and conversion devices including Zn-based batteries and energy-efficient water electrolysis for hydrogen production.

potential values were calculated using the equation: $E_{RHE} = E_{Hg/HgO} + 0.0591\ pH + 0.098$.

The Zn–NO_3^- battery was assembled with CoO/CuO-NA/CF ($1 \times 1\ cm^2$) as the cathode and a polished Zn plate ($1 \times 1\ cm^2$) as the anode. A typical H-type cell that contained 30 mL of the cathode electrolyte (0.5 M NaOH contained with 500 ppm NO_3^-–N) and 30 mL of the anode electrolyte (6 M KOH) was separated using the Nafion 117 membrane. Zn–NO_3^- battery was tested under an Ar atmosphere at room temperature using an Autolab electrochemical workstation (Nova 2.1). Electrochemical impedance spectroscopy (EIS) was performed at an open-circuit potential state in the frequency range from 10^6 Hz to 0.01 Hz with a voltage amplitude of 10 mV.

2.4. Ammonia detection

The NH_3 concentration was determined by colorimetry using the indophenol blue method.[50] In detail, 2 mL of 1 M NaOH coloring solution containing 5% salicylic acid and 5% sodium citrate, 1 mL oxidizing solution of 0.05 M NaClO, and 0.2 mL catalyst solution of $Na_2Fe(CN)_5NO{\cdot}2H_2O$ (1 wt%) were added to 2 mL of the electrolyte after electrolysis. After standing in the dark for 2 h, UV-vis absorption spectra were measured. The concentration of NH_3 was estimated using the absorbance at a wavelength of 653 nm. The concentration-absorbance curve was calibrated using the standard NH_4Cl-N solution with concentrations of 0, 0.5, 1.0, 1.5, 2.0, and 2.5 ppm in 0.5 M NaOH solution.

2.5. Determination of FE and NH_3 yield

FE_{NH3} is defined as the amount of the electric charge used for synthesizing NH_3 divided by the total charge passed through the electrode during electrolysis. The total amount of NH_3 yield was measured using colorimetry, the indophenol blue method. FE and yield toward NH_3 *via* NO_3RR were calculated using the following equation:

$$FE = (8 \times F \times C \times V)/(17 \times Q) \times 100\%$$

The NH_3 yield was calculated using the following equation:

$$NH_3\ \text{yield} = (C \times V)/(17 \times t \times A)$$

where F is the faradaic constant (96 485 C mol^{-1}), C is the concentration of measured NH_3, V is the volume of electrolyte in the cathode chamber (30 mL), 17 is the molar mass of NH_3, Q is the total quantity of applied electricity, t is the electrolysis time, and A is the loaded area of catalyst ($1 \times 1\ cm^2$).

3. Results and discussion

3.1. Material preparation and characterization

As shown in Fig. 1a, CoO/CuO-NA/CF was synthesized through a three-step process, which included anodic oxidation, electrodeposition, and the annealing process. After the anodic oxidation process, CF was converted to sky-blue ($Cu(OH)_2$-NA/CF).[37] The Co element was regularly distributed on $Cu(OH)_2$-NA/CF by the subsequent electrodeposition process. After annealing, CoO/CuO-NA/CF was obtained (Fig. S1, ESI,† see Experimental section for more details). The surface topography of the catalyst was studied by scanning electron microscopy (SEM) analysis. SEM images of the original CF revealed that the surface of the untreated copper foam is smooth without any nanoarray structures (Fig. S2, ESI†). After anodizing and annealing treatments, nanoarray structures were formed on the surface of copper oxide (Fig. 1b).[37] By electrodeposition and annealing, CoO/CuO-NA/CF was prepared (Fig. 1c). The high-resolution transmission electron microscopy (HRTEM) image of CoO/CuO-NA/CF, shown in Fig. 1d, confirms the heterogeneous interface between the CoO and CuO domains. The lattice fringes of 0.24 nm and 0.25 nm are corresponding to CoO (111) and CuO (111) crystalline planes, respectively. The heterogeneous interface between the CoO and CuO domains marked by the dotted line can be clearly observed.[51,52] Fig. 1e shows the HAADF-STEM image and the corresponding elemental mapping of a representative CoO/CuO-NA/CF. It can be seen that Cu, Co, and O elements are homogeneously distributed on CoO/CuO-NA/CF. The energy dispersive X-ray (EDX) spectrum also shows the simultaneous presence of Cu, Co, and O (Fig. S3, ESI†). Through the EDX-mapping test, the Cu : Co atomic ratio was estimated as 51 : 2. The X-ray diffractometer (XRD) pattern (Fig. S4, ESI†) shows that the diffraction peaks of Cu at 43.29°, 50.43°, and 74.13° corresponded to the crystal planes of (111), (200), and (220) (PDF# 04-0836).[53] The characteristic peaks of CuO-NA/CF and CoO/CuO-NA/CF at 35.6° and 38.9° correspond to CuO (PDF# 74-1021). Fig. S5† shows the XRD patterns of Co–$Cu(OH)_2$ and CoO/CuO-NA/CF. The pattern of Co–$Cu(OH)_2$ corresponds well to $Cu(OH)_2$ (PDF# 80-0656). There were no obvious peaks of Co species, which may be due to its low content or low crystallinity.[54] After the annealing of Co–$Cu(OH)_2$, corresponding characteristic peaks of CoO (PDF# 75-0393) and CuO (PDF# 74-1021) were observed in the XRD pattern of CoO/CuO-NA/CF. This confirmed the simultaneous existence of CoO and CuO, which is consistent with the HRTEM results shown in Fig. 1d.

In order to investigate the electronic structure of the materials, X-ray photoelectron spectroscopy (XPS) was conducted. Fig. S6† shows the XPS survey spectrum of the samples, confirming the presence of Co, Cu, and O elements in CoO/CuO-NA/CF. The appearance of O in CF may be due to surface oxidation when it is exposed to air.[55] Fig. 1f shows the Cu 2p XPS spectra of CF, CuO-NA/CF, and CoO/CuO-NA/CF. The Cu 2p spectrum of CF displays four peaks at 932.6, 952.5, 935.0, and 955.0 eV, which can be assigned to Cu^0 $2p_{3/2}$, Cu^0 $2p_{1/2}$, Cu^{2+} $2p_{3/2}$, and Cu^{2+} $2p_{1/2}$, respectively.[56] The peaks at 943.7 and 962.3 eV are satellite peaks present in all electrode materials.[56] For CuO-NA/CF, the XPS analysis of Cu 2p showed peaks of 933.6 eV for Cu $2p_{3/2}$ and 953.4 eV for Cu $2p_{1/2}$ of CuO species, which is consistent with previous reports.[51] After CoO was introduced, the Cu 2p spectrum of CoO/CuO-NA/CF exhibited two typical peaks at 933.8 and 953.6 eV, which are attributed to Cu^{2+} $2p_{3/2}$ and Cu^{2+} $2p_{1/2}$, respectively. The binding energy of Cu $2p_{3/2}$ and Cu $2p_{1/2}$ of CoO/CuO-NA/CF have a shift of about 0.2 eV compared to that of CuO-NA/CF,

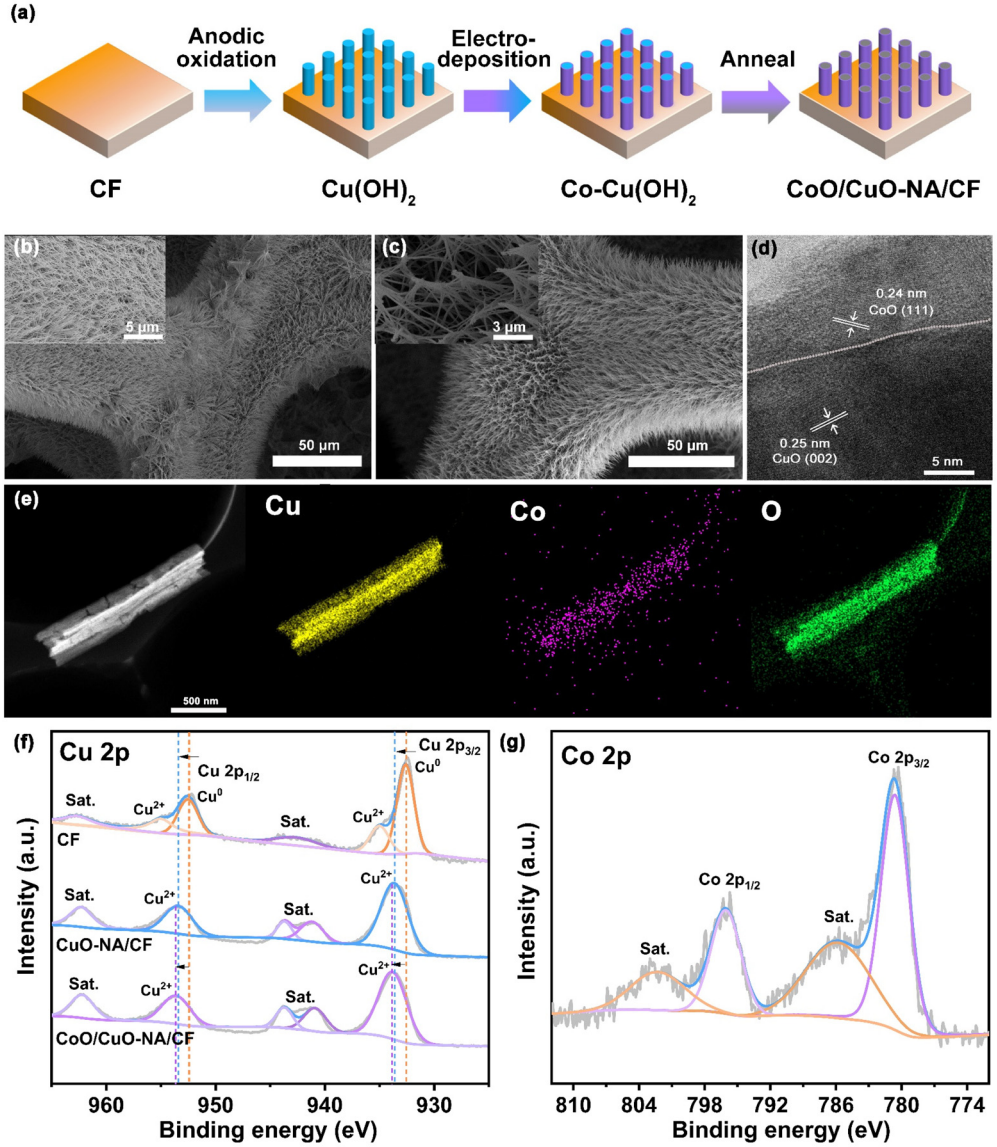

Fig. 1 (a) Schematic illustration for CoO/CuO-NA/CF synthesis. (b) SEM images of CuO-NA/CF. (c) SEM images of CoO/CuO-NA/CF. (d) High-resolution TEM images of CoO/CuO-NA/CF. (e) The HAADF-STEM image and EDX mappings corresponding to Cu, Co, and O elements in CoO/CuO-NA/CF. (f) Cu 2p XPS spectra of CF, CuO-NA/CF, and CoO/CuO-NA/CF. (g) Co 2p XPS spectra of CoO/CuO-NA/CF.

which is possibly attributed to the interaction between CoO and Cu components in CoO/CuO-NA/CF.[55] Fig. 1g shows the Co 2p XPS spectra of CoO/CuO-NA/CF. The two peaks of 780.6 and 796.1 eV correspond to Co $2p_{3/2}$ and Co $2p_{1/2}$, respectively, and satellite peaks appearing at positions of 785.8 and 802.3 eV, confirmed that Co was present in the form of Co^{2+}.[57,58] In addition, the changes in the O1s peak and Cu LMM AES spectra of CF, CuO-NA/CF, and CoO/CuO-NA/CF also indicated the effect of CoO/CuO on changes in the electronic properties (Fig. S7, ESI†).[37]

3.2. Electrocatalytic NO_3RR performance

In order to confirm the effect of CoO on the electrocatalytic activity of Cu-based oxides, the NO_3RR performance of the catalyst was evaluated using an H-type cell. Fig. 2a compares the linear sweeping voltammetry (LSV) curves of CF, CuO-NA/CF, and CoO/CuO-NA/CF at 0.5 M NaOH (with or without 250 ppm of NO_3^-–N) for NO_3RR. It is worth noting that the reduction current using the CoO/CuO-NA/CF catalyst is higher than that with CF and CuO-NA/CF catalysts.[59] Electrochemical impedance spectroscopy (EIS) was used to investigate the transfer resistance of the electrode interfaces.[60] As shown in Fig. S8,† CoO/CuO-NA/CF exhibited a smaller semicircle, which further highlights good conductivity and low interfacial charge transfer resistance.[61–63] In addition, we conducted the electrochemical surface area (ECSA) measurements of Cu, CuO-NA/CF, and CoO/CuO-NA/CF. The obtained order of C_{dl} for the electrodes (CoO/CuO-NA/CF (6.94 mF) > CuO-NA/CF

(5.07 mF) > CF (2.54 mF)) showed that the transformation from the smooth Cu surface to the 3D morphology of the modified electrodes significantly increased the active surface area (Fig. S9, ESI†). As shown in Fig. S10,† CoO/CuO-NA/CF exhibits a significantly increased current density in an electrolyte containing NO_3^-, confirming its capability to catalyze NO_3RR. To investigate the activity and selectivity of the catalyst for NO_3RR, the constant voltage method was used to characterize the performance, using the indophenol blue method to detect the concentration of NH_3 generated in the solution (Fig. S11–S13, ESI†).[64,65] Both CF, CuO-NA/CF, and CoO/CuO-NA/CF showed an increase in NH_3 yield with more negative potential, and CoO/CuO-NA/CF showed higher NH_3 yield and FE (Fig. 2b and c). The highest NH_3 yields of CF and CuO-NA/CF were 147.3 and 196.4 μmol h^{-1} cm^{-2}, respectively, and CoO/CuO-NA/CF could reach 296.9 μmol h^{-1} cm^{-2} at −0.7 V *vs.* RHE. CoO/CuO-NA/CF showed the highest FE of NH_3 at 92.9%, and the NH_3 yield was 83.3 μmol h^{-1} cm^{-2} at −0.2 V *vs.* RHE. For CF and CuO-NA/CF, FEs were 61.8% and 85.1% at −0.2 V *vs.* RHE, respectively. Due to the competitive hydrogen evolution reaction, FE decreases as the potential shifts negatively.

In addition, the CoO/CuO-NA/CF stability tests were performed at −0.2 V *vs.* RHE and the catalysts remained stable for 16 cycles (Fig. 2d). The time-current curve, the number of transferred electrons, and the UV-vis test curves for cyclic testing are shown in Fig. S14, ESI.† Fig. 2e also shows that the yield of NH_3 in the pre-electrolysis solution and pure NaOH was negligible, proving that NH_3 was obtained by NO_3^- reduction. At the same time, isotope labeling experiments were carried out with $^{14}NO_3^-$ and $^{15}NO_3^-$ as nitrogen sources.[66] The ^1H NMR spectrum of the $^{14}NO_3^-/^{15}NO_3^-$ aqueous solution after electrolysis showed typical trimodal/bimodal, which is consistent with that of the standard $^{14}NH_4^+/^{15}NH_4^+$ sample (Fig. 2f), confirming that the NH_3 detected in the electrolyte comes from the nitrogen sources $^{14}NO_3^-/^{15}NO_3^-$. NMR quantification of $^{14}NH_4^+$ was also performed (see ESI, Fig. S14† for details), and the resulting quantification of $^{14}NH_4^+$ was close to that determined by UV-vis (Fig. 2e and Fig. S15, ESI†), which confirmed the accuracy of the various quantification methods for NH_3.

To understand more about the active components of the catalyst before and after electrochemical NO_3RR, various surface characterization methods were tried. XRD, XPS, and AES tests were performed on the catalysts after electrochemical reduction. The XRD pattern (Fig. 3a) showed that the catalysts still exhibited strong peaks for Cu metal and CuO and CoO after the reaction. After the electrochemical reaction, Cu^{2+} species from CuO were partially converted into Cu^0 and Cu^+, causing a weakening of the CuO peak strength. In the Cu 2p XPS spectra (Fig. 3b), the original Cu 2p peaks belonged to Cu^{2+}. After the electrochemical reduction, the peaks at 934.6

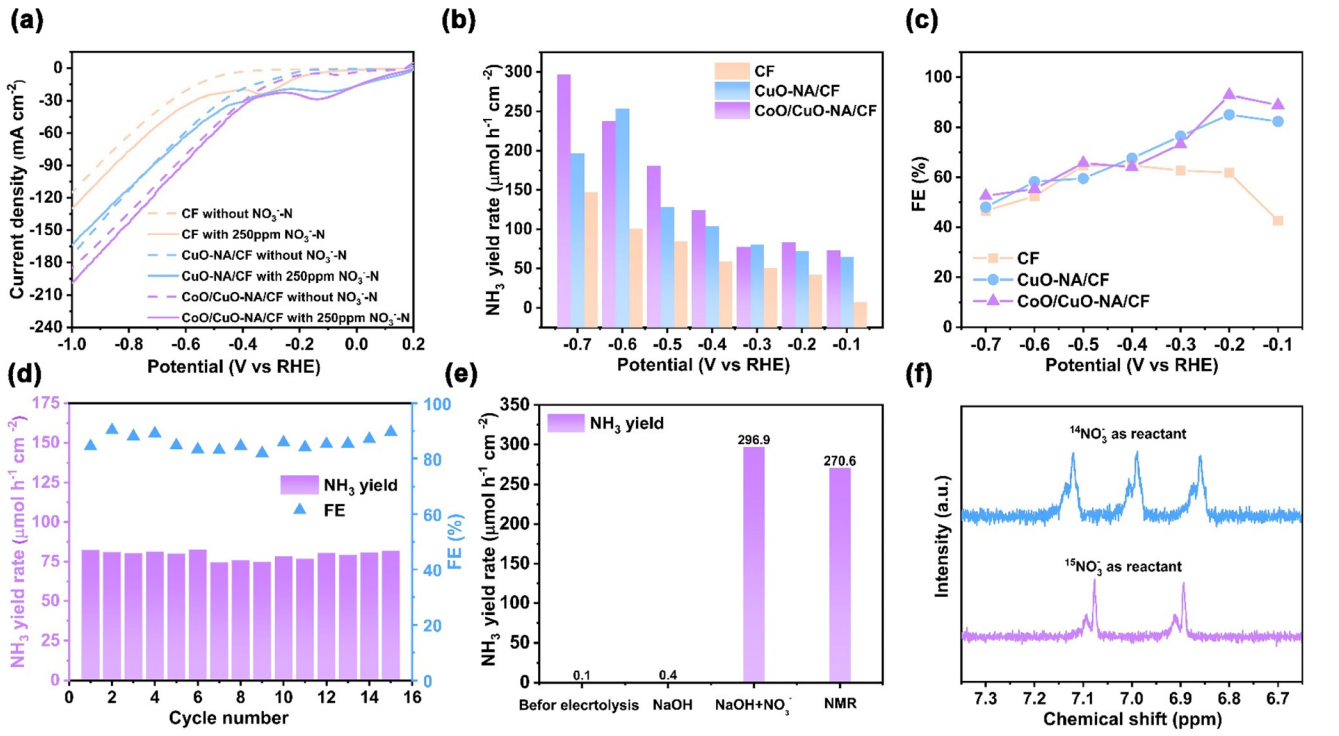

Fig. 2 (a) LSV curves of CF, CuO-NA/CF, and CoO/CuO-NA/CF in 0.5 M NaOH (with and without 250 ppm NO_3^-–N). (b and c) NH_3 yields and FEs of CF, CuO-NA/CF, and CoO/CuO-NA/CF at different given potentials. (d) NH_3 yields and FEs of CoO/CuO-NA/CF during the recycling test at −0.2 V *vs.* RHE. (e) The amount of the produced NH_3 under different conditions for CoO/CuO-NA/CF. (f) ^1H NMR spectra of the electrolytes after NO_3RR using $^{14}NO_3^-$–N and $^{15}NO_3^-$–N for CoO/CuO-NA/CF.

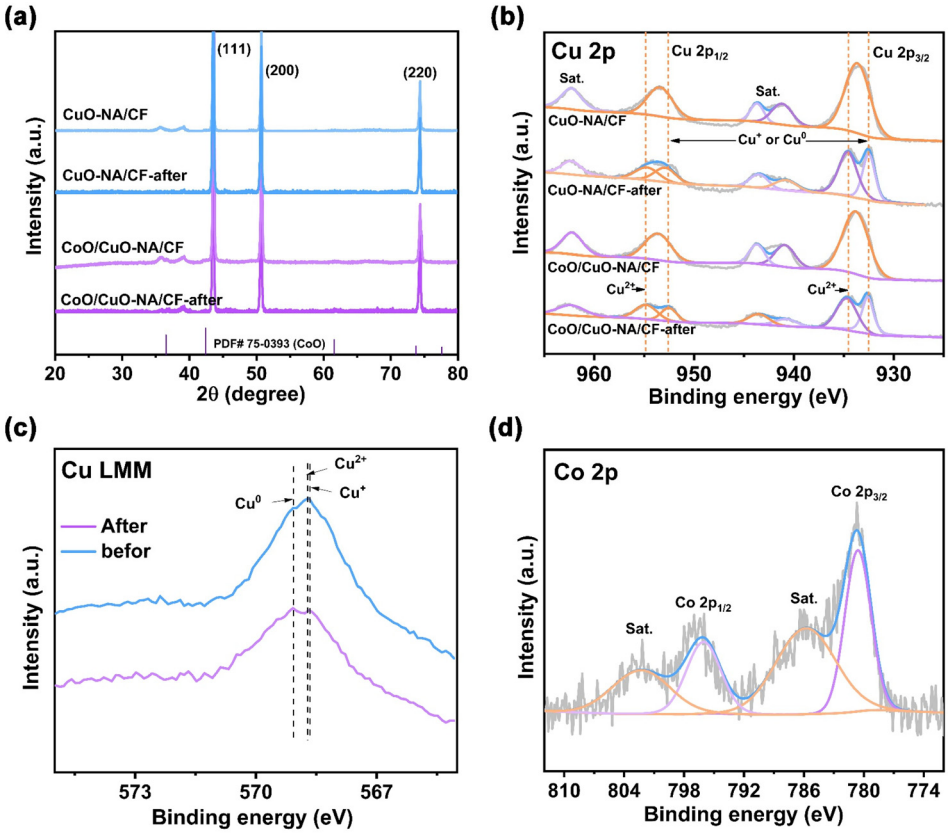

Fig. 3 Comparison of (a) XRD and (b) Cu 2p XPS spectra for CuO-NA/CF and CoO/CuO-NA/CF before and after NO_3RR. (c) Auger Cu LMM spectra for CoO/CuO-NA/CF before and after NO_3RR. (d) Co 2p XPS spectra of CoO/CuO-NA/CF after NO_3RR.

eV and 954.7 eV can be attributed to Cu^{2+}, at the same time, Cu^+ or Cu^0 peaks appeared at approximately 932.5 eV (Cu $2p_{3/2}$) and 952.9 eV (Cu $2p_{1/2}$).[67] In addition, Cu LMM AES spectroscopy was utilized to distinguish between Cu^+ and Cu^0 (Fig. 3c). Cu^{2+} (568.8 eV) splits into two peaks after the electrochemical reduction, belonging to the characteristic Auger peaks of Cu^0 (569.1 eV) and Cu^+ (568.6 eV).[37] Overall, after the electrochemical reaction, a part of Cu^{2+} was converted into Cu^0/Cu^+ to form the active Cu/Cu_2O phase, which promoted NO_3RR, consistent with previous reports.[37,68,69] In addition, the Co 2p XPS result showed that Co existed in the 2+ oxidation state (Fig. 3d).

The active phase Cu/Cu_2O tended to promote the NO_3RR process through the electron transfer reduction pathway, which has good adsorption capacity for nitrate but suffers from weaker hydrogen adsorption. The Co^{2+} in the heterostructure promotes the adsorption of H* and synergistically enhances the nitrate reduction of the active phase Cu/Cu_2O,[70] which can overcome the disadvantages of poor stability of Cu electrodes. The promotional effect of Co^{2+} for H* adsorption and nitrate reduction ultimately leads to the enhancement of NO_3RR performance. Combined with electrochemical testing results, it is shown that the CuO phase will transform into Cu^0/Cu^+ states during the reaction process, and CoO sites have a promoting effect on the NO_3RR of CuO-NA/CF.

3.3. Zn–NO_3^- battery performance of CoO/CuO-NA/CF

After confirming that CoO/CuO-NA/CF is an excellent catalyst for nitrate reduction to ammonia, we further assembled the aqueous Zn–NO_3^- battery system by using CoO/CuO-NA/CF as the cathode and Zn plate as the anode (Fig. 4a). Fig. 4b shows the charge and discharge polarization curves of CuO-NA/CFand CoO/CuO-NA/CF-based Zn–NO_3^- battery. CoO/CuO-NA/CF-based Zn–NO_3^- battery has a lower charge–discharge potential difference compared to CuO-NA/CF. The power density of the CoO/CuO-NA/CF-based Zn–NO_3^- battery peaked at 4.3 mW cm^{-2}, which was higher than that of the CuO-NA/CF-based Zn–NO_3^- battery (Fig. 4c). As shown in Fig. 4d, both CuO-NA/CF and CoO/CuO-NA/CF-based Zn–NO_3^- batteries exhibited an open circuit potential of 1.1 V relative to Zn/Zn^{2+}, and CuO-NA/CF-based Zn–NO_3^- battery had a more obvious attenuation trend. In addition, the CoO/CuO-NA/CF-based Zn–NO_3^- battery is capable of lighting the LED bulb.

Fig. 4e shows the discharge curves of the Zn-NO_3^- battery at different currents, ranging from 4 mA cm^{-2} to 14 mA cm^{-2}. Additionally, our CoO/CuO-NA/CF-based Zn–NO_3^- battery exhibited an advantageous FE and yield of NH_3 for NO_3RR compared to other reported catalysts (Fig. 4f and Table S1†). Fig. 4g shows the NH_3 yield and the corresponding FE when discharged at different output current densities. The CoO/

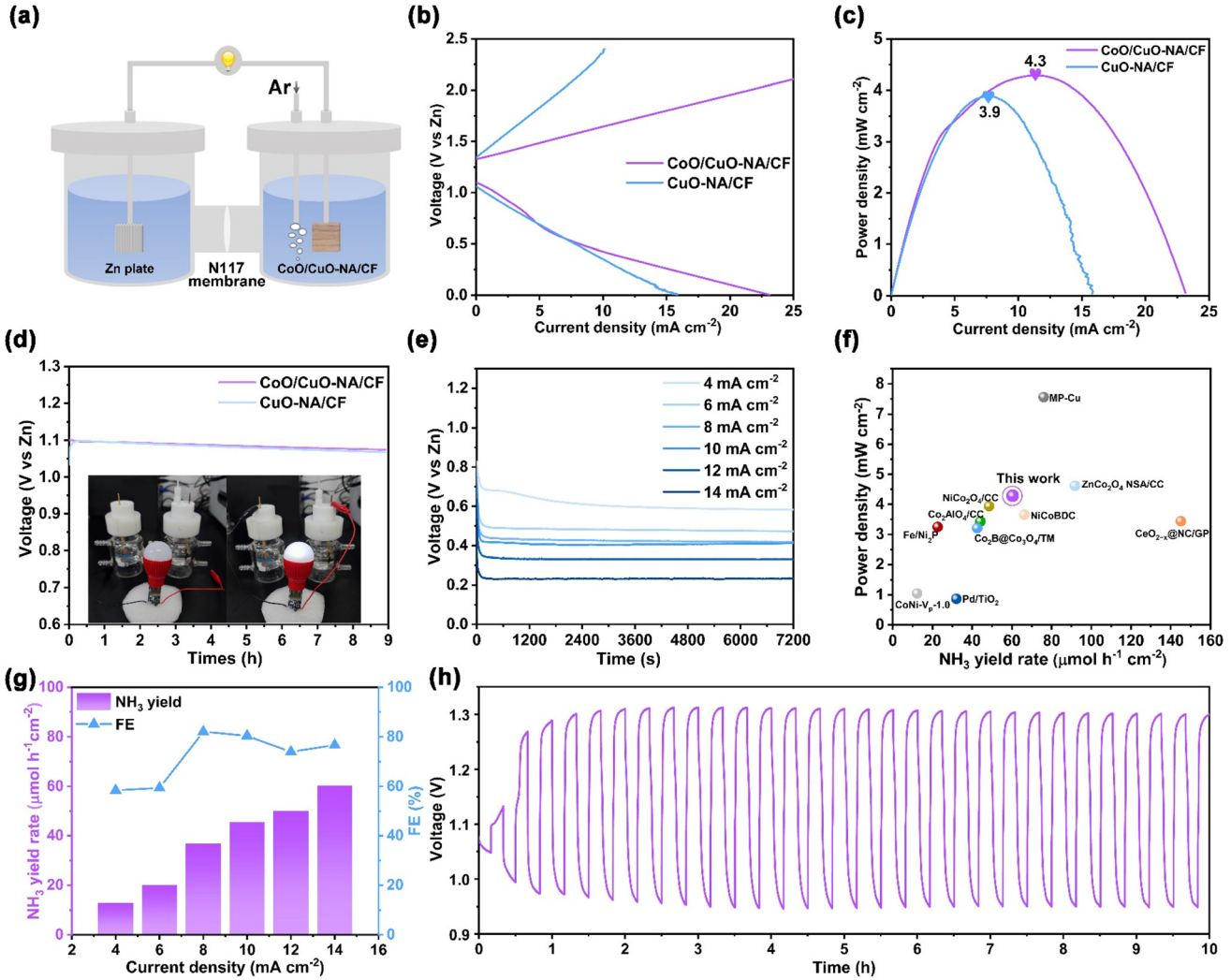

Fig. 4 (a) Schematic diagram of the Zn–NO_3^- battery. The Zn–NO_3^- battery using CuO-NA/CF and CoO/CuO-NA/CF catalysts as a cathode: (b) discharge and charge polarization curves, (c) power density, and (d) open-circuit voltage and digital graph of a white LED bulb illuminated by a Zn–NO_3^- battery. (e) Discharge curves at different current densities. (f) Power density and NH_3 yield of CoO/CuO-NA/CF-based Zn–NO_3^- battery in comparison to other reported Zn–NO_3^- batteries. The CoO/CuO-NA/CF-based Zn–NO_3^- battery: (g) NH_3 yields and corresponding FEs at various current densities, and (h) galvanostatic discharge–charge cycling curves at 0.5 mA cm^{-2}.

CuO-NA/CF-based Zn–NO_3^- battery provides the highest NH_3 yield of 60.3 μmol h^{-1} cm^{-2} at 14 mA cm^{-2} and achieves the highest FE of 82.0% at 8 mA cm^{-2}. In contrast, the CuO-NA/CF-based Zn–NO_3^- battery showed a poor NH_3 yield and corresponding FE at each current density (Fig. S16, ESI†). In addition, the charge–discharge cycle curves of the CoO/CuO-NA/CF-based Zn–NO_3^- battery were tested. The anode undergoes the dissolution and deposition of Zn during discharge and charging, respectively. The cathode undergoes the reduction of nitrate to ammonia during discharge, and an oxygen evolution reaction (OER) occurs during charging (Fig. S17, ESI†). Fig. 4h shows the discharge–charge process of the Zn–NO_3^- battery at a constant current density of 5 mA cm^{-2}, and it was stable over a long cycle of 10 h. The above results show that our CoO/CuO-NA/CF-based Zn–NO_3^- battery has good performance, and the heterostructured CoO/CuO-NA/CF can distinctly improve the performance of the individual species of CuO-NA/CF, whether it is a NO_3RR or Zn–NO_3^- battery.

4. Conclusion

In summary, a heterostructured CoO/CuO nanoarray electrocatalyst was successfully fabricated for high-efficiency NO_3RR toward NH_3 synthesis and Zn–NO_3^- battery. The rationally designed CoO/CuO-NA/CF electrode showed higher catalytic activity than the primary CF and CuO-NA/CF and reached a maximum NH_3 yield of 296.9 μmol h^{-1} cm^{-2} and the highest FE of 92.9%. Furthermore, by integrating the CoO/CuO-NA/CF cathode with a Zn plate anode, a Zn–NO_3^- battery simultaneously generated electricity, and synthesized NH_3 from

NO_3RR. Specifically, the CoO/CuO-NA/CF-based Zn–NO_3^- battery delivered a power density of 4.3 mW cm^{-2} with an FE of 82.0% and yield of 60.3 μmol h^{-1} cm^{-2} for NH_3 production and showed stable charge–discharge cycling of 10 h. This work provides a promising heterostructure catalyst for green NH_3 production while generating electricity.

Conflicts of interest

The authors declare no competing financial interest.

Acknowledgements

This work was financially supported by the National Natural Science Foundation of China (22075211, 51971157, and 22275166), Shenzhen Science and Technology Programs (JCYJ20210324123202008, JCYJ20210324115412035 and ZDSYS20210813095534001), Guangdong Foundation for Basic and Applied Basic Research Program (2021A1515110880) and Tianjin Science Fund for Distinguished Young Scholars (19JCJQJC61800).

References

1 K. H. R. Rouwenhorst, Y. Engelmann, K. van 't Veer, R. S. Postma, A. Bogaerts and L. Lefferts, *Green Chem.*, 2020, **22**, 6258–6287.
2 G. Zhang, X. Li, K. Chen, Y. Guo, D. Ma and K. Chu, *Angew. Chem., Int. Ed.*, 2023, **62**, 202300054.
3 A. Chen and B. Y. Xia, *J. Mater. Chem. A*, 2019, **7**, 23416–23431.
4 F. Jiao and B. Xu, *Adv. Mater.*, 2019, **31**, 1805173.
5 T. Wu, W. Fan, Y. Zhang and F. Zhang, *Mater. Today Phys.*, 2021, **16**, 100310.
6 Q. Liu, L. Xie, J. Liang, Y. Ren, Y. Wang, L. Zhang, L. Yue, T. Li, Y. Luo, N. Li, B. Tang, Y. Liu, S. Gao, A. A. Alshehri, I. Shakir, P. O. Agboola, Q. Kong, Q. Wang, D. Ma and X. Sun, *Small*, 2022, **18**, 2106961.
7 D. Qi, F. Lv, T. Wei, M. Jin, G. Meng, S. Zhang, Q. Liu, W. Liu, D. Ma, M. S. Hamdy, J. Luo and X. Liu, *Nano Res. Energy*, 2022, **1**, 9120022.
8 X. Li, T. Li, Y. Ma, Q. Wei, W. Qiu, H. Guo, X. Shi, P. Zhang, A. M. Asiri, L. Chen, B. Tang and X. Sun, *Adv. Energy Mater.*, 2018, **8**, 1801357.
9 X. Li, K. Chen, X. Lu, D. Ma and K. Chu, *Chem. Eng. J.*, 2023, **454**, 140333.
10 H. Wang, F. Zhang, M. Jin, D. Zhao, X. Fan, Z. Li, Y. Luo, D. Zheng, T. Li, Y. Wang, B. Ying, S. Sun, Q. Liu, X. Liu and X. Sun, *Mater. Today Phys.*, 2023, **30**, 100944.
11 J. Ding, X. Hou, Y. Qiu, S. Zhang, Q. Liu, J. Luo and X. Liu, *Inorg. Chem. Commun.*, 2023, **151**, 110621.
12 S. Chen, K. Lian, W. Liu, Q. Liu, G. Qi, J. Luo and X. Liu, *Nano Res.*, 2023, **16**, 9214–9230.
13 X. Zhang, Y. Wang, C. Liu, Y. Yu, S. Lu and B. Zhang, *Chem. Eng. J.*, 2021, **403**, 126269.
14 R. Zhang, Z. Wu, Z. Huang, Y. Guo, S. Zhang, Y. Zhao and C. Zhi, *Chin. Chem. Lett.*, 2022, **34**, 107600.
15 P. H. van Langevelde, I. Katsounaros and M. T. M. Koper, *Joule*, 2021, **5**, 290–294.
16 M. Teng, J. Ye, C. Wan, G. He and H. Chen, *Ind. Eng. Chem. Res.*, 2022, **61**, 14731–14746.
17 Z. Li, Z. Deng, L. Ouyang, X. Fan, L. Zhang, S. Sun, Q. Liu, A. A. Alshehri, Y. Luo, Q. Kong and X. Sun, *Nano Res.*, 2022, **15**, 8914–8921.
18 H. Liu, X. Lang, C. Zhu, J. Timoshenko, M. Ruscher, L. Bai, N. Guijarro, H. Yin, Y. Peng, J. Li, Z. Liu, W. Wang, B. R. Cuenya and J. Luo, *Angew. Chem., Int. Ed.*, 2022, **61**, 202202556.
19 Y. Gao, K. Wang, C. Xu, H. Fang, H. Yu, H. Zhang, S. Li, C. Li and F. Huang, *Appl. Catal. B*, 2023, **330**, 122627.
20 M. Yang, J. Sun, Y. Qin, H. Yang, S. Zhang, X. Liu and J. Luo, *Sci. China Mater.*, 2022, **65**, 536–542.
21 H. Shen, T. Wei, Q. Liu, S. Zhang, J. Luo and X. Liu, *J. Colloid Interface Sci.*, 2023, **634**, 730–736.
22 S. Liu, L. Wang, H. Yang, S. Gao, Y. Liu, S. Zhang, Y. Chen, X. Liu and J. Luo, *Small*, 2022, **18**, 2104965.
23 Q. Zhang, K. Lian, Q. Liu, G. Qi, S. Zhang, J. Luo and X. Liu, *J. Colloid Interface Sci.*, 2023, **646**, 844–854.
24 W. Liu, W. Que, R. Yin, J. Dai, D. Zheng, J. Feng, X. Xu, F. Wu, W. Shi, X. Liu and X. Cao, *Appl. Catal. B*, 2023, **328**, 122488.
25 W. Liu, X. Niu, J. Feng, R. Yin, S. Ma, W. Que, J. Dai, J. Tang, F. Wu, W. Shi, X. Liu and X. Cao, *ACS Appl. Mater. Interfaces*, 2023, **15**, 15344–15352.
26 H. Gu, W. Yue, J. Hu, X. Niu, H. Tang, F. Qin, Y. Li, Q. Yan, X. Liu, W. Xu, Z. Sun, Q. Liu, W. Yan, L. Zheng, Y. Wang, H. Wang, X. Li, L. Zhang, G. Xia and W. Chen, *Adv. Energy Mater.*, 2023, **13**, 2204014.
27 H. Shang, Z. Jiang, D. Zhou, J. Pei, Y. Wang, J. Dong, X. Zheng, J. Zhang and W. Chen, *Chem. Sci.*, 2020, **11**, 5994–5999.
28 Y. J. Qin and J. Luo, *Chem. J. Chin. Univ.*, 2022, **43**, 20220300.
29 T. Wang, Q. Zhang, K. Lian, G. Qi, Q. Liu, L. Feng, G. Hu, J. Luo and X. Liu, *J. Colloid Interface Sci.*, 2023, **655**, 176–186.
30 H. Shang, X. Zhou, J. Dong, A. Li, X. Zhao, Q. Liu, Y. Lin, J. Pei, Z. Li, Z. Jiang, D. Zhou, L. Zheng, Y. Wang, J. Zhou, Z. Yang, R. Cao, R. Sarangi, T. Sun, X. Yang, X. Zheng, W. Yan, Z. Zhuang, J. Li, W. Chen, D. Wang, J. Zhang and Y. Li, *Nat. Commun.*, 2020, **11**, 3049.
31 L. Ji, X. Peng and Z. Wang, *Trans. Tianjin Univ.*, 2020, **26**, 373–381.
32 P. V. Shinde, R. Samal and C. S. Rout, *Trans. Tianjin Univ.*, 2022, **28**, 80–88.
33 J. Zhou, F. Pan, Q. Yao, Y. Zhu, H. Ma, J. Niu and J. Xie, *Appl. Catal. B*, 2022, **317**, 121811.
34 D. Qi, Y. Liu, M. Hu, X. Peng, Y. Qiu, S. Zhang, W. Liu, H. Li, G. Hu, L. Zhuo, Y. Qin, J. He, G. Qi, J. Sun, J. Luo and X. Liu, *Small*, 2020, **16**, 2004855.

35 T. Wu, X. Kong, S. Tong, Y. Chen, J. Liu, Y. Tang, X. Yang, Y. Chen and P. Wan, *Appl. Surf. Sci.*, 2019, **489**, 321–329.
36 X. Zhang, C. Wang, Y. Guo, B. Zhang, Y. Wang and Y. Yu, *J. Mater. Chem. A*, 2022, **10**, 6448–6453.
37 Y. Wang, W. Zhou, R. Jia, Y. Yu and B. Zhang, *Angew. Chem., Int. Ed.*, 2020, **59**, 5350–5354.
38 W. Yu, J. Yu, M. Huang, Y. Wang, Y. Wang, J. Li, H. Liu and W. Zhou, *Energy Environ. Sci.*, 2023, **16**, 2991–3001.
39 Z. Chang, G. Meng, Y. Chen, C. Chen, S. Han, P. Wu, L. Zhu, H. Tian, F. Kong, M. Wang, X. Cui and J. Shi, *Adv. Mater.*, 2023, 2304508.
40 K. Chen, Z. Ma, X. Li, J. Kang, D. Ma and K. Chu, *Adv. Funct. Mater.*, 2023, **33**, 2209890.
41 Q. Li, R. Deng, Y. Chen, J. Gong, P. Wang, Q. Zheng, Y. Huo, F. Xie, X. Wei, C. Yang and D. Lin, *Small*, 2023, **19**, 2303642.
42 S. Liu, L. Kang and S. C. Jun, *Adv. Mater.*, 2021, **33**, 2004689.
43 Y. Liu, X.-M. Yao, X. Liu, Z. Liu and Y.-Q. Wang, *Inorg. Chem.*, 2023, **62**, 7525–7532.
44 Z. Deng, C. Ma, X. Fan, Z. Li, Y. Luo, S. Sun, D. Zheng, Q. Liu, J. Du, Q. Lu, B. Zheng and X. Sun, *Mater. Today Phys.*, 2022, **28**, 100854.
45 X. Fan, C. Liu, Z. Li, Z. Cai, L. Ouyang, Z. Li, X. He, Y. Luo, D. Zheng, S. Sun, Y. Wang, B. Ying, Q. Liu, A. Farouk, M. S. Hamdy, F. Gong, X. Sun and Y. Zheng, *Small*, 2023, **19**, 2303424.
46 C. Li, K. Li, C. Chen, Q. Tang, T. Sun and J. Jia, *Sep. Purif. Technol.*, 2020, **237**, 116485.
47 Z. Niu, S. Fan, X. Li, P. Wang, Z. Liu, J. Wang, C. Bai and D. Zhang, *Chem. Eng. J.*, 2022, **450**, 138343.
48 T. Wang, S. Gao, T. Wei, Y. Qin, S. Zhang, J. Ding, Q. Liu, J. Luo and X. Liu, *Chem. – Eur. J.*, 2023, **29**, 202204034.
49 J. Hou, X. Peng, J. Sun, S. Zhang, Q. Liu, X. Wang, J. Luo and X. Liu, *Inorg. Chem. Front.*, 2022, **9**, 3047–3058.
50 Z. Deng, J. Liang, Q. Liu, C. Ma, L. Xie, L. Yue, Y. Ren, T. Li, Y. Luo, N. Li, B. Tang, A. A. Alshehri, I. Shakir, P. O. Agboola, S. Yan, B. Zheng, J. Du, Q. Kong and X. Sun, *Chem. Eng. J.*, 2022, **435**, 135104.
51 X. Xiong, C. You, Z. Liu, A. M. Asiri and X. Sun, *ACS Sustainable Chem. Eng.*, 2018, **6**, 2883–2887.
52 X. Wu, Z. Zhang, C. He, Y. Shen, X. Wu, H. Wang, Z. Ma and Q. Li, *Chem. Eng. J.*, 2023, **453**, 139831.
53 Y. Liu, B. Deng, K. Li, H. Wang, Y. Sun and F. Dong, *J. Colloid Interface Sci.*, 2022, **614**, 405–414.
54 M. Ghosh, M. Ibrar and J. M. Smith, *Chem. Commun.*, 2022, **58**, 4783–4786.
55 N. K. Tyagi, B. K. Mahapatra, S. Ghimire, N. Manna, D. Kumar, V. Kumar, K. Mukhopadhyay and S. K. Singh, *ACS Appl. Energy Mater.*, 2023, **6**, 6111–6119.
56 J. Y. Fang, Q. Z. Zheng, Y. Y. Lou, K. M. Zhao, S. N. Hu, G. Li, O. Akdim, X. Y. Huang and S. G. Sun, *Nat. Commun.*, 2022, **13**, 7899.
57 Y. Lan, H. Luo, Y. Ma, Y. Hua, T. Liao and J. Yang, *Nanoscale*, 2021, **13**, 10108–10115.
58 S. Liu, L. Kang, J. Zhang, E. Jung, S. Lee and S. C. Jun, *Energy Storage Mater.*, 2020, **32**, 167–177.
59 Z. Jiang, S. Song, X. Zheng, X. Liang, Z. Li, H. Gu, Z. Li, Y. Wang, S. Liu, W. Chen, D. Wang and Y. Li, *J. Am. Chem. Soc.*, 2022, **144**, 19619–19626.
60 S. Liu, L. Kang, J. Zhang, S. C. Jun and Y. Yamauchi, *ACS Energy Lett.*, 2021, **6**, 4127–4154.
61 S. Gao, S. Chen, Q. Liu, S. Zhang, G. Qi, J. Luo and X. Liu, *ACS Appl. Nano Mater.*, 2022, **5**, 12387–12394.
62 S. Liu, M. Jin, J. Sun, Y. Qin, S. Gao, Y. Chen, S. Zhang, J. Luo and X. Liu, *Chem. Eng. J.*, 2022, **437**, 135294.
63 X. Peng, R. Zhang, Y. Mi, H.-T. Wang, Y.-C. Huang, L. Han, A. R. Head, C.-W. Pao, X. Liu, C.-L. Dong, Q. Liu, S. Zhang, W.-F. Pong, J. Luo and H. L. Xin, *ChemSusChem*, 2023, **16**, 202201385.
64 G. Wang, Y. Zhang, K. Chen, Y. Guo and K. Chu, *Inorg. Chem.*, 2023, **62**, 6570–6575.
65 Y. Zhang, X. Chen, W. Wang, L. Yin and J. C. Crittenden, *Appl. Catal. B*, 2022, **310**, 121346.
66 Z. Wang, C. Sun, X. Bai, Z. Wang, X. Yu, X. Tong, Z. Wang, H. Zhang, H. Pang, L. Zhou, W. Wu, Y. Liang, A. Khosla and Z. Zhao, *ACS Appl. Mater. Interfaces*, 2022, **14**, 30969–30978.
67 J. Kim, W. Choi, J. W. Park, C. Kim, M. Kim and H. Song, *J. Am. Chem. Soc.*, 2019, **141**, 6986–6994.
68 W. Liu, P. Zhai, A. Li, B. Wei, K. Si, Y. Wei, X. Wang, G. Zhu, Q. Chen, X. Gu, R. Zhang, W. Zhou and Y. Gong, *Nat. Commun.*, 2022, **13**, 1877.
69 M. Wang, H. Chen, M. Wang, J. Wang, Y. Tuo, W. Li, S. Zhou, L. Kong, G. Liu, L. Jiang and G. Wang, *Angew. Chem., Int. Ed.*, 2023, **62**, 202306456.
70 H. Liu, J. Li, F. Du, L. Yang, S. Huang, J. Gao, C. Li and C. Guo, *Green Energy Environ.*, 2023, **8**, 1619–1629.